ЖЭТФ, 2024, том 166, вып. 5 (11), стр. 688–695

FRACTIONAL A. C. JOSEPHSON EFFECT AS EVIDENCE OF TOPOLOGICAL HINGE STATES IN A DIRAC SEMIMETAL $NiTe_2$

D. Yu. Kazmin, V. D. Esin, A. V. Timonina, N. N. Kolesnikov, E. V. Deviatov*

Institute of Solid State Physics of the Russian Academy of Sciences
142432, Chernogolovka, Moscow District, Russia

Received April 25, 2024
revised version July 3, 2024
Accepted for publication July 4, 2024

We experimentally investigate Josephson current between two 5 μm spaced superconducting indium leads, coupled to a $NiTe_2$ single crystal flake, which is a type-II Dirac semimetal. Under microwave irradiation, we demonstrate a. c. Josephson effect at millikelvin temperatures as a number of Shapiro steps. In addition to the integer ($n = 1, 2, 3, 4, ...$) steps, we observe fractional ones at half-integer values $n = 1/2, 3/2, 5/2$ and 7/2, which corresponds to π periodicity of current-phase relationship. In contrast to previous investigations, we do not observe 4π periodicity (disappearance of the odd $n = 1, 3, 5, ...$ Shapiro steps), while the latter is usually considered as a fingerprint of helical surface states in Dirac semimetals and topological insulators. We argue, that our experiment confirms Josephson current through the topological hinge states in $NiTe_2$: since one can exclude bulk supercurrent in 5 μm long Josephson junctions, interference of the hinge modes is responsible for the π periodicity, while stable odd Shapiro steps reflect chiral character of the topological hinge states.

DOI: 10.31857/S0044451024110117

1. INTRODUCTION

Like other topological materials [1–5], topological semimetals acquire topologically protected surface states due to the bulk-boundary correspondence (as a recent review see [6]). In contrast to topological insulators, Dirac semimetals are characterized by gapless bulk spectrum with band touching in some distinct Dirac points. In Weyl semimetals every touching point splits into two Weyl nodes with opposite chiralities. Fermi arc surface states are connecting projections of these nodes on the surface Brillouin zone, so the topological surface states are chiral for Weyl materials [6]. For Dirac semimetals, the surface states are helical, similarly to topological insulators [1].

The main problem of transport investigations is to reveal the surface states contribution in topological semimetals with gapless bulk spectrum [6]. In proximity with a superconductor, topological surface (or edge) states are able to carry supercurrents over extremely large distances [7–13], while the coherence length is much smaller for the bulk carriers. Also, nonuniform supercurrent distribution is reflected in d. c. or a. c. Josephson effect. For example, it may lead to the superconducting quantum interference device (squid)-like critical current suppression pattern [8,14,15] and/or to the fractional a. c. Josephson effect [9,16,17] with half-integer Shapiro steps.

For the typical Dirac semimetal Cd_3As_2, observation of π and 4π periodic current-phase relationship has been reported in Al-Cd_3As_2-Al and Nb-Cd_3As_2-Nb junctions [13,16]. For the short 100 nm junctions, the fractional a. c. Josephson effect (π periodicity) is connected with interference between the bulk and surface supercurrent contributions [16], while the disappearance of $n = 1$ Shapiro step (4π periodicity) reflects the helical nature of topological surface states in Dirac semimetals also for 1 μm long junctions [13].

Recently it has been understood, that besides the well-known three-dimensional bulk Dirac states and the two-dimensional Fermi-arc surface states, there should be one-dimensional hinge states [18] at the intersections between surfaces of Dirac semimetals [19, 20]. Dirac semimetals exhibit hinge states as universal, direct consequences of their bulk three-dimensional Dirac points, see Ref. [18] for details. These hinge states represent a new kind of Chern-type insulator edge states, so they are chiral even for Dirac semimetals [18,19]. The idea

* E-mail: dev@issp.ac.ru

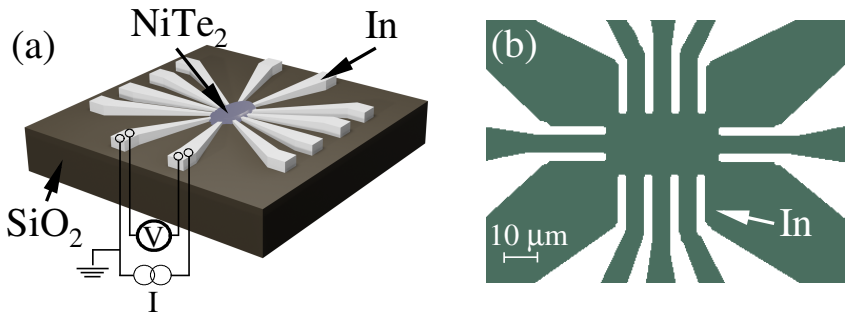

Fig. 1. (Color online) *a* — A sketch of a sample with In leads and external electrical connections. A thick (above 0.5 μm) $NiTe_2$ mechanically exfoliated flake is placed on the pre-defined In leads pattern to form 5 μm separated In-$NiTe_2$-In junctions. Electron transport is investigated between two neighbor superconducting indium leads in a four-point technique, all the wire resistances are excluded. *b* — An optical image of the indium leads pattern before transferring the $NiTe_2$ single crystal flake

of the experiment [21] is to distinguish between different types of current-carrying states since the coherence length should be longer in the one-dimensional hinge channel than that in the surface and bulk ones. As a result, standard Fraunhofer interference pattern in a short Josephson junction is changed to the squid-like one for the 1 μm long Cd_3As_2 based junctions [21], because the supercurrent is dominated by several hinge channels in the latter case.

Due to the topological origin, the effect should also be independent on the particular material. $NiTe_2$ is a recently discovered type-II Dirac semimetal belonging to the family of transition metal dichalcogenides. Nontrivial topology of $NiTe_2$ single crystals has been confirmed by spin-resolved ARPES [22, 23]. The bulk coherence length ξ is smaller in $NiTe_2$ in comparison with Cd_3As_2 due to the smaller mean free path l_e, which should further suppress the bulk supercurrent. The contribution from the topological surface states reveals itself as the Josephson diode effect in parallel magnetic field [24, 25].

Similarly to Cd_3As_2 Dirac material, hinge states have been theoretically predicted [26] in $NiTe_2$. Hinge supercurrent has been demonstrated in the submicron-size $NiTe_2$ based Josephson junction as a (squid)-like critical current suppression pattern due to the magnetic field suppression of the bulk supercurrent [26]. Thus, it is reasonable to study a. c. Josephson effect in long $NiTe_2$ junctions to confirm topological (chiral) nature of the predicted hinge states in Dirac semimetals.

Here, we experimentally investigate Josephson current between two 5 μm spaced superconducting indium leads, coupled to a $NiTe_2$ single crystal flake, which is a type-II Dirac semimetal. Under microwave irradiation, we demonstrate a. c. Josephson effect at millikelvin temperatures as a number of Shapiro steps. In addition to the integer ($n = 1, 2, 3, 4, ...$) steps, we observe fractional ones at half-integer values $n = 1/2, 3/2, 5/2$ and $7/2$, which corresponds to π periodicity of current-phase relationship. In contrast to previous investigations, we do not observe 4π periodicity (disappearance of the odd $n = 1, 3, 5, ...$ Shapiro steps).

2. SAMPLES AND TECHNIQUE

$NiTe_2$ was synthesized from elements, which were taken in the form of foil (Ni) and pellets (Te). The mixture was heated in an evacuated silica ampule up to 815° C with the rate of 20 deg/h, the ampule was kept at this temperature for 48 h. The crystal was grown in the same ampule by the gradient freezing technique with the cooling rate of 10 deg/h. As a result, we obtain 80 mm long and 5 mm thick $NiTe_2$ single crystal, with (0001) cleavage plane.

The powder X-ray diffraction analysis (Cu Kα1 radiation, $\lambda = 1.540598$ Å) confirms single-phase $NiTe_2$ with P-3m1 (164) space group (a = b = 3.8791 Å, c = 5.3005 Å), see Fig. 1 *a*. The known structure model is also refined with single crystal X-ray diffraction measurements (Oxford diffraction Gemini-A, Mo Kα). Nearly stoichiometric ratio $Ni_{1-x}Te_2$ ($x < 0.06$) is verified by the energy-dispersive X-ray spectroscopy.

The quality of our $NiTe_2$ material was also tested in standard four-point magnetoresistance measurements, see Ref. [25] for details. In particular, nonsaturating longitudinal magnetoresistance [27, 28] was confirmed for our $NiTe_2$ samples in normal magnetic field [25]. It is important, that four-point resistance is finite (0.1 Ω) between two 5 μm spaced Au leads in zero magnetic field, so there is no bulk superconductivity [29] for

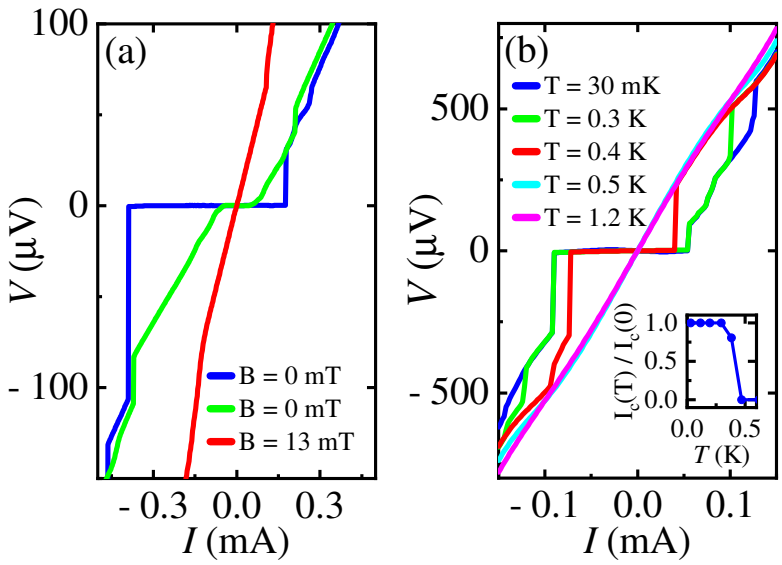

Fig. 2. (Color online) Standard Josephson $I-V$ characteristics for three different In-$NiTe_2$-In samples with different critical currents and normal resistances (blue and green curves in (*a*), blue curve in (*b*)), obtained at 30 mK temperature in zero magnetic field. The current sweep direction is from the positive to negative currents, which is the origing of $I-V$ asymmetry. Suppression of the zero-resistance state is shown in (*a*) for $B = 13$ mT normal to the plane magnetic field (red curve) at 30 mK temperature and in (*b*) for different temperatures in zero field. Inset shows the normalized critical current temperature dependence $I_c(T)/I_c(0)$

$NiTe_2$ single crystal flakes at ambient pressure even at millikelvin temperatures [25].

Fig. 1 *a* shows a sketch of a sample. Despite $NiTe_2$ can be thinned down to two-dimensional monolayers, topological semimetals are essentially three-dimensional objects [6]. Thus, we have to select relatively thick (above 0.5 μm) $NiTe_2$ single crystal flakes, which also ensures sample homogeneity.

Thick flakes require special contact preparation technique: the In leads pattern is firstly formed on a standard oxidized silicon substrate by lift-off, as depicted in Fig. 1 *b*. The 100 nm thick In leads are separated by 5 μm intervals, which defines the experimental geometry. As a second step, the fresh mechanically exfoliated $NiTe_2$ flake is transferred to the In leads pattern and is shortly pressed to the leads by another oxidized silicon substrate, the latter is removed afterward. The substrates are kept strictly parallel by external metallic frame to avoid sliding of the $NiTe_2$ crystal, which is verified in optical microscope. As a result, planar In-$NiTe_2$ junctions are formed at the bottom surface of the $NiTe_2$ single crystal flake in Fig. 1 *a*, being separated by 5 μm intervals, as depicted in Fig. 1 *b*. As an additional advantage, the In-$NiTe_2$ junctions and the surface between them are protected from any contamination by SiO_2 substrate, since they are placed at the bottom side of a thick $NiTe_2$ flake in Fig. 1 *a*.

This procedure provides transparent In-$NiTe_2$ junctions, stable in different cooling cycles, which has been verified before for a wide range of materials [8, 9, 11, 25, 30, 31]. Thus, they are suitable to form long In-$NiTe_2$-In SNS structures. The mean free path l_e can be estimated as $l_e \approx 4$ μm in $NiTe_2$ from the four-point resistance [25], so it is smaller than the $L = 5\mu$m intervals between indium leads in Fig. 1. L should be compared [32, 33] with the coherence length of the diffusive SNS junction

$$\xi = (l_e \hbar v_F^N / \pi \Delta_{in})^{1/2} \approx 300\,\text{nm},$$

where Fermi velocity is $v_F^N \approx 10^7\,\text{cm/s}$, and $\Delta_{In} = 0.5$ meV is the indium superconducting gap [34]. Due to the obvious relation $L/\xi > 10$, one can not expect bulk Josephson current in our $L = 5\mu$m long In-$NiTe_2$-In SNS structures. This estimation well corresponds to the results of Ref. [25], where there was no bulk contribution to the supercurrent on the pristine $NiTe_2$ surface between two 1 μm spaced superconducting leads.

We study electron transport between two superconducting indium leads in a four-point technique. An example of electrical connections is shown in Fig. 1 *a*: one In electrode is grounded, the current I is fed through the neighboring one; a voltage drop V is measured between these two indium electrodes by independent wires. In this connection scheme, all the wire

resistances are excluded, which is necessary for low-impedance In-$NiTe_2$-In junctions (0.25–5 Ohm normal resistance in the present experiment).

The indium leads are superconducting below the critical temperature [34] $T_c \approx 3.4\ K$. However, we observe Josephson current only below 1 K, so the measurements are performed in a dilution refrigerator with 30 mK base temperature. For a. c. Josephson effect investigations, the sample is illuminated by microwave (rf) radiation through an open coaxial line. Due to specifics of the dilution frige, we have to restrict rf radiation by 0.5 GHz frequency and 7 dBm power, the bath temperature is always below 60 mK in this case.

3. EXPERIMENTAL RESULTS

To obtain $I-V$ characteristics, we sweep the d. c. current I and measure the voltage drop V, see $I-V$ curves in Fig. 2 for three different samples. The normal In-$NiTe_2$-In junction resistance varies from $\approx 0.2\ \Omega$ in (a) to $5\ \Omega$ in (b), due to the different overlap between the $NiTe_2$ flake and In leads for different samples.

In zero magnetic field and at low 30 mK temperature, Fig. 2 shows standard Josephson behavior, despite of $L >> \xi$ for the present In-$NiTe_2$-In junctions: (i) by the four-point connection scheme we directly demonstrate zero resistance region at low currents. (ii) The non-zero resistance appears as sharp jumps at current values $I_c \approx 0.05 - 0.4$ mA for different samples. The current sweep direction is from the positive to negative currents, so the cricical Josephson current is characterized by left (negative) $I-V$ branch. The obtained I_c values are much smaller than the critical current for the indium leads, which can be estimated as ≈ 30 mA for the leads' dimensions and the known [35] indium critical current density $j \approx 3 \cdot 10^6 \mathrm{A/cm}^2$. (iii) $I-V$ curve can be switched to standard Ohmic behavior, if the supercurrent is suppressed by magnetic field (13 mT) or temperature (above 0.5 K), see (a) and (b), respectively.

Inset to Fig. 2 b shows the normalized critical current temperature dependence $I_c(T)$, which is unusual for long $L > \xi$ diffusive $L >> l_e$ SNS junctions [32,33]. On the other hand, one can not expect bulk Josephson current for $L/\xi > 10$ for our In-$NiTe_2$-In structures, while the topological surface states carry the Josephson current in Refs. [24–26] probably due to the backscattering suppression.

The main experimental finding is the observation of fractional a. c. Josephson effect with π periodicity of the current-phase relationship.

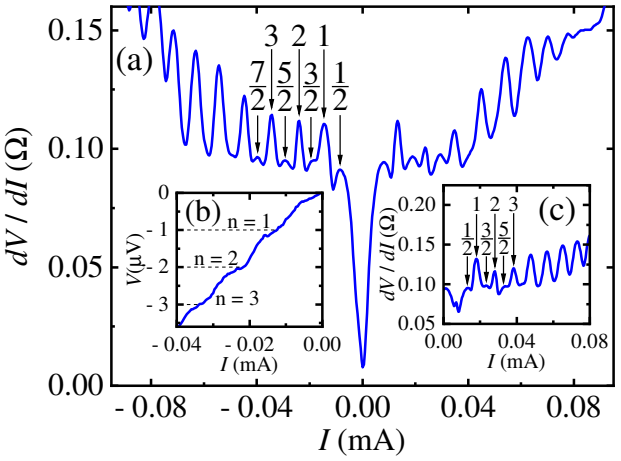

Fig. 3. (Color online) Differential $dV/dI(I)$ characteristics of the In-$NiTe_2$-In junctions under rf (0.5 GHz, 7 bBm) irradiation through an open coaxial line. The data are obtained in zero magnetic field, the sample temperature is always below 60 mK. Shapiro steps with integer numbers $n = 1, 2, 3, 4, ...$ can be seen as sharp equidistant dV/dI peaks. We check, that the peaks well correspond to the centers of the steps in usual d. c. $I-V$ curves (e.g., in the left inset, where Shapiro steps at $V = nhf/2e$ levels are depicted by dashed lines). In addition to the integer steps, there are fractional ones at $n = 1/2, 3/2, 5/2$ and 7/2 as small dV/dI peaks, some $dV/dI(I)$ asymmetry is connected with the current sweep direction. Right inset shows qualitatively similar $dV/dI(I)$ behavior with half-integer Shapiro steps for another sample, so the main experimental finding is the observation of fractional a. c. Josephson effect with π periodicity of the current-phase relationship

Differential $dV/dI(I)$ characteristics under rf irradiation are shown in in Fig. 3. Dilution fridge restricts radiation frequency (0.5 GHz) and power (7 dBm) to avoid sample overheating through the coaxial lines. The power at the sample is unknown, but the base temperature is always below 60 mK under irradiation. In these conditions, $dV/dI(I)$ curves allows to increase resolution of Shapiro steps in Fig. 3: the d. c. current I is additionally modulated by a low (100 nA) a. c. component, the a. c. ($\sim dV/dI$) voltage is measured by a lock-in amplifier. The signal is confirmed to be independent of the modulation frequency within 100 Hz – 10kHz range, which is defined by the applied filters.

Shapiro steps with integer numbers $n = 1, 2, 3, 4, ...$ can be seen as sharp equidistant dV/dI peaks, see the main field of Fig. 3. We check, that they are the peaks which well correspond to the centers of the steps in usual d. c. $I-V$ curves, see the left inset to Fig. 3. Thus, we should concentrate on the peaks (not dips) while considering differential $dV/dI(I)$ char-

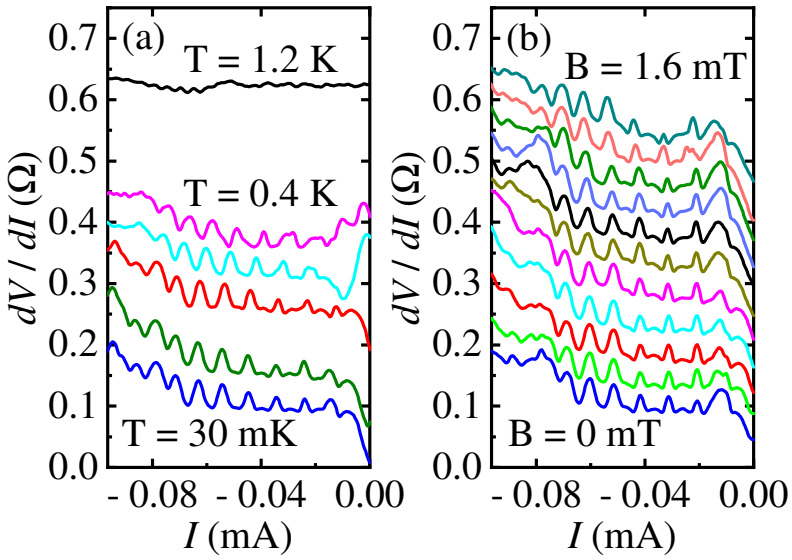

Fig. 4. (Color online) Integer and half-integer dV/dI peaks for different temperatures (30 mK, 0.1 K, 0.2 K, 0.3 K, 0.4 K and 1.2 K) (*a*) and magnetic fields (from 0 to 1.6 mT with .16 mT step) (*b*). Shapiro steps are not sensitive to low $B << B_c \approx 13$ mT magnetic fields in (*b*), while they are moving to lower currents above 200 mK and disappear above 0.4 K in (*a*), the half-integer steps disappear earlier. This behavior principally reflects the Josephson supercurrent behavior, as it can be expected for Shapiro steps. **Magnetic field is normal to the sample plane in (*b*)**

acteristics, probably due to the imperfect steps' shape at low frequency and power. Shapiro steps are placed at $V = nhf/2e$ in the inset to Fig. 3, as it should be expected for typical SNS junctions with trivial 2π periodicity in current-phase relationship $I_J \sim \sin(\phi)$.

In addition to the integer steps, we observe small but clearly visible fractional ones at $n = 1/2, 3/2, 5/2$ and $7/2$ as small dV/dI peaks. The peaks appear at low currents I, they can be seen both for positive and negative currents. Some $dV/dI(I)$ asymmetry is connected with the current sweep direction from the positive to negative current values, so the right $dV/dI(I)$ branch is obtained while sweeping from the resistive sample state. Thus, we demonstrate π periodicity of the current-phase relationship for the fractional a. c. Josephson effect in long In-$NiTe_2$-In junctions.

This behavior is well-reproducible for different samples, e.g. $dV/dI(I)$ curve under rf irradiation is presented in the right inset to Fig. 3 with integer and half-integer Shapiro steps. It is important, that this reproducibility is inconsistent with sample fabrication defects, e.g. parasite shorting of In leads. As additional arguments against fabrication defects, the thickness of the indium film is chosen to be much smaller than the leads separation (100 nm$<<$ 5μm) to avoid parasite shortings. The zero-field critical current values for the present In-$NiTe_2$-In junctions well correspond to ones in Ref. [25], despite different materials of the superconducting leads. Josephson effect is fully suppressed above 0.5 K and at 13 mT magnetic field in Fig. 2, which is also far below the values for pure indium [34]. Thus, we should conclude that long In-$NiTe_2$-In junctions show half-integer steps (π periodicity of the current-phase relationship) due to the properties of $NiTe_2$ Dirac semimetal.

The step positions are stable at low temperatures in Fig. 4 *a*, while they are moving to lower currents above 200 mK and disappear above 0.4 K. dV/dI peaks are also not sensitive to low $B << B_c \approx 13$ mT magnetic fields, see Fig. 4 *b*. This behavior principally reflects the critical current I_c behavior in Fig. 2, as it can be expected for Shapiro steps. The half-integer steps disappear earlier in Fig. 4 *a*.

4. DISCUSSION

First of all, there is no bulk superconductivity [29] for $NiTe_2$ single crystal flakes at ambient pressure even at millikelvin temperatures. Bulk superconductivity is known for pressurized Te-deficient $NiTe_2$ [29], but it can be ruled out in our case, since (i) bulk superconductivity is not observed for our $NiTe_2$ crystals according to four-point resistance data in Ref [25]; (ii) X-ray spectroscopy reveals almost stoichiometric $Ni_{1-x}Te_2$ crystal

with a slight Ni deficiency ($x < 0.06$); (iii) there is no external pressure in the present experiment.

On the other hand, topological surface states carry the Josephson current on the pristine $NiTe_2$ surface [24–26]. Because of topological protection, surface states can efficiently transfer the Josephson current, which is reflected in slow $I_c(T)$ decay in the inset to Fig. 2 *b*. In this case, it is quite natural to observe integer Shapiro steps at $V = nhf/2e$, as it should be expected for typical SNS junctions with trivial 2π periodicity in current-phase relationship $I_J \sim sin(\phi)$.

The specifics of our In-$NiTe_2$-In junctions is the fact, that we do not observe 4π periodicity in a. c. Josephson effect: the integer $n = 1$ Shapiro step is as strong as the $n = 2$ in Fig. 3, while the maximum rf power value covers the range of $n = 1$ disappearance in Refs. [13, 16]. Moreover, the even sequence of Shapiro steps is usually observed [38] when frequency is below 1 GHz, similarly to our experiment. 4π periodicity is connected with the helical nature [6] of topological surface states in Dirac semimetals [13, 16] and topological insulators [38]. Thus, we should explain both the presence of π periodicity and why we do not see 4π one in comparison with [13, 16].

As the main experimental finding, fractional a. c. Josephson effect with π periodicity of the current-phase relationship appears as half-integer $n = 1/2, 3/2, 5/2$ and $7/2$ Shapiro steps. For standard SNS junctions, higher weak-link transparency results in a more skewed current-phase relationship [17, 36, 37], which is usually the origin of half-integer Shapiro steps. For our long $\xi << L$ junctions, one could expect that it is high electron mobility in topological surface states that leads to skewed current-phase relationship [37].

Even in this case, one should expect inteference between one-dimensional channels [39–43], which, for example, appears for nontrivial Josephson current distribution in topological materials [9, 16, 17]. Recently, π-periodic $sin(2\phi)$ current-phase relationship has been predicted and experimentally demonstrated for different realizations of superconducting quantum interference devices [44–46]. For short Cd_3As_2 Dirac semimetal junctions [13,16], interference (π periodicity) could appear if both surface and bulk carriers transferred Josephson current in parallel.

Each conduction channel, including the bulk Dirac fermions, Fermi-arc surface states, and topological hinge states, can be distinguished based on their different superconducting coherence lengths by increasing the channel length of the Josephson junction. In our case, one cannot expect [32, 33] the bulk Josephson current for 5 μm long In-$NiTe_2$-In junctions, because of small bulk coherence length $\xi << L$. Helical surface states can transfer Josephson current for 1 μm distance [25], while it is much smaller than $L = 5$ μm for our In-$NiTe_2$-In junctions. Also, we do not observe 4π periodicity, which is the fingerprint of helical surface states.

On the other hand, hinge states [19, 20] have been theoretically predicted [26] and experimentally demonstrated [26] in $NiTe_2$ type-II Dirac semimetal. Interference of the hinge modes can explain all our observations: Josephson current for unprecidingly long In-$NiTe_2$-In junctions, and observation of π periodicity without the 4π one. (i) The coherence length should be longer in the one-dimensional hinge channel than that in the surface and bulk states, giving rise to the supercurrent being dominated by the hinge channels in long Josephson junctions [21]. (ii) For one-dimensional hinge states, one can expect interference of supercurrent through the states localized at the intersections between surfaces, i.e. fractional a. c. Josephson effect with π periodicity [39–43]. (iii) Topological hinge states inherit the chiral property of the Chern insulator edge states [18, 19], so they should not demonstrate 4π periodicity of the current-phase relationship.

Thus, our experiment can be considered not only as demonstration of transport through the topological hinge states in $NiTe_2$ Dirac semimetal, but also as the confirmation of their chiral property.

5. CONCLUSION

As a conclusion, we experimentally investigate Josephson current between two 5 μm spaced superconducting indium leads, coupled to a $NiTe_2$ single crystal flake, which is a type-II Dirac semimetal. Under microwave irradiation, we demonstrate a. c. Josephson effect at millikelvin temperatures as a number of Shapiro steps. In addition to the integer ($n = 1, 2, 3, 4, ...$) steps, we observe fractional ones at half-integer values $n = 1/2, 3/2, 5/2$ and $7/2$, which corresponds to π periodicity of current-phase relationship. In contrast to previous investigations, we do not observe 4π periodicity (disappearance of the odd $n = 1, 3, 5, ...$ Shapiro steps), while the latter is usually considered as a fingerprint of helical surface states in Dirac semimetals and topological insulators. We argue, that our experiment confirms Josephson current through the topological hinge states in $NiTe_2$: since one can exclude bulk supercurrent in 5 μm long Josephson junctions, interference of the hinge modes is responsible for the π periodicity, while stable odd Shapiro steps reflect chiral character of the topological hinge states.

Acknowledgments. We wish to thank S. S. Khasanov for X-ray sample characterization, and A. N. Nekrasov for the energy-dispersive X-ray spectroscopy. We gratefully acknowledge financial support by the RF State task.

REFERENCES

1. B. A. Volkov and O. A. Pankratov, JETP Lett. **42**, 178 (1985).

2. M. Z. Hasan and C. L. Kane, Rev. Mod. Phys. **82**, 3045 (2010).

3. X.-L. Qi and S.-C. Zhang, Rev. Mod. Phys. **83**, 1057 (2011).

4. A. Bansil, H. Lin, and T. Das, Rev. Mod. Phys. **88**, 021004 (2016).

5. C.-K. Chiu, J. C. Teo, A. P. Schnyder, and S. Ryu, Rev. Mod. Phys. **88**, 035005 (2016).

6. N. P. Armitage, E. J. Mele, and A. Vishwanath, Rev. Mod. Phys. **90**, 15001 (2018).

7. J. H. Lee, G.-H. Lee, J. Park, J. Lee, S.-G. Nam, Y.-S. Shin, J. S. Kim, and H.-J. Lee, Nano Lett. **14**, 5029 (2014).

8. O. O. Shvetsov, A. Kononov, A. V. Timonina, N. N. Kolesnikov, and E. V. Deviatov, JETP Lett. **107**, 774 (2018).

9. O. O. Shvetsov, A. Kononov, A. V. Timonina, N. N. Kolesnikov, and E. V. Deviatov, EP **124**, 47003 (2018).

10. C. Huang, B. T. Zhou, H. Zhang, B. Yang, R. Liu, H. Wang, Y. Wan, K. Huang, Z. Liao, E. Zhang, S. Liu, Q. Deng, Y. Chen, X. Han, J. Zou, X. Lin, Z. Han, Y. Wang, K. Tuen Law, and F. Xiu, Nat. Comm. **10**, 2217 (2019).

11. O. O. Shvetsov, V. D. Esin, Yu. S. Barash, A. V. Timonina, N. N. Kolesnikov, and E. V. Deviatov, Phys. Rev. B **101**, 035304 (2020).

12. Y. Wang, S. Yang, P. K. Sivakumar, B. R. Ortiz, S. M. L. Teicher, H. Wu, A. K. Srivastava, C. Garg, D. Liu, S. S. P. Parkin, E. S. Toberer, T. McQueen, S. D. Wilson, and M. N. Ali, arXiv:2012.05898. Sci.Adv.9, eadg7269 (2023), DOI:10.1126/sciadv.adg7269

13. Cai-Zhen Li, Chuan Li, Li-Xian Wang, Shuo Wang, Zhi-Min Liao, Alexander Brinkman, and Da-Peng Yu, Phys. Rev. B **97**, 115446 (2018), DOI:10.1103/PhysRevB.97.115446

14. S. Hart, H. Ren, T. Wagner, P. Leubner, M. Mühlbauer, C. Brüe, H. Buhmann, L. W. Molenkamp, and A. Yacoby, Nature Physics **10**, 638 (2014), DOI:10.1038/nphys3036

15. V. S. Pribiag, A. J. A. Beukman, Fanming Qu, M. C. Cassidy, C. Charpentier, W. Wegscheider, and L. P. Kouwenhoven, Nature Nanotechnology **10**, 593 (2015).

16. W. Yu, W. Pan, D. L. Medlin, M. A. Rodriguez, S.R. Lee, Z. Bao, and F. Zhang, Phys. Rev. Lett. **120**, 177704 (2018), DOI:10.1103/PhysRevLett.120.177704

17. R. A. Snyder, C. J. Trimble, C. C. Rong, P. A. Folkes, P. J. Taylor, and J. R. Williams, Phys. Rev. Lett. **121**, 097701 (2018), DOI:10.1103/PhysRevLett.121.097701

18. B. J. Wieder, Zhijun Wang, J. Cano, B. Bradlyn, and B. A. Bernevig, Nature Commun. **11**, 627 (2020), DOI:10.1038/s41467-020-14443-5

19. W. A. Benalcazar, B. A. Bernevig, and T. L. Hughes, Phys. Rev. B **96**, 245115 (2017).

20. D. Calugaru, V. Juricic, and B. Roy, Phys. Rev. B **99**, 041301 (2019).

21. Cai-Zhen Li, An-Qi Wang, Chuan Li, Wen-Zhuang Zheng, A. Brinkman, Da-Peng Yu, and Zhi-Min, Liao Phys. Rev. Lett. **124**, 156601 (2020)

22. B. Ghosh, D. Mondal, C.-N. Kuo, C. S. Lue, J. Nayak, J. Fujii, I. Vobornik, A. Politano, and A. Agarwal, Phys. Rev. B **100**, 195134 (2019).

23. S. Mukherjee, S. W. Jung, S. F. Weber, C. Xu, D. Qian, X. Xu, P. K. Biswas, T. K. Kim, L. C. Chapon, M. D. Watson, J. B. Neaton, and C. Cacho, Sci. Rep. **10**, 12957 (2020)

24. B. Pal, A. Chakraborty, P. K. Sivakumar, M. Davydova, A. K. Gopi, A. K. Pandeya, J. A. Krieger, Yang Zhang, M. Date, Sailong Ju, Noah Yuan, N. B. M. Schröter, Liang Fu, and S. S. P. Parkin, Nat. Phys. **18**, 1228 (2022), DOI:10.1038/s41567-022-01699-5

25. V. D. Esin, O. O. Shvetsov, A. V. Timonina, N. N. Kolesnikov, and E. V. Deviatov, Nanomaterials **12**, 4114 (2022), DOI:10.3390/nano12234114

26. Tian Le, Ruihan Zhang, Changcun Li, Ruiyang Jiang, Haohao Sheng, Linfeng Tu, Xuewei Cao, Zhaozheng Lyu, Jie Shen, Guangtong Liu, Fucai Liu, Zhijun Wang, Li Lu, and Fanming Qu, Nature Commun. 2785 (2024), arXiv:2303.05041, DOI:10.1038/s41467-024-47103-z

27. C. Xu, B. Li, W. Jiao, W. Zhou, B. Qian, R. Sankar, N. D. Zhigadlo, Y. Qi, D. Qian, F.-C. Chou, and X. Xu, Chem. Mater. **30**, 4823 (2018).

28. Q. Liu, F. Fei, B. Chen, X. Bo, B. Wei, S. Zhang, M. Zhang, F. Xie, M. Naveed, X. Wan, F. Song, and B. Wang, Phys. Rev. B **99**, 155119 (2019).

29. Z. Feng, J. Si, T. Li, H. Dong, C. Xu, J. Yang, Z. Zhang, K. Wang, H. Wu, Q. Hou, J.-J. Xing, S. Wan, S. Li, W. Deng, J. Feng, A. Pal, F. Chen, S. Hu, J.-Y. Ge, C. Dong, S. Wang, W. Ren, S. Cao, Y. Liu, X. Xu, J. Zhang, B. Chen, and N.-C. Yeh, Materials Today Phys. **17**, 100339 (2021).

30. O. O. Shvetsov, Yu. S. Barash, A. V. Timonina, N. N. Kolesnikov, and E. V. Deviatov, JETP Let. **115**, 267 (2022), DOI:10.1134/S0021364022100101

31. V. D. Esin, D. Yu. Kazmin, Yu. S. Barash, A. V. Timonina, N. N. Kolesnikov, and E. V. Deviatov, JETP Lett. **118**, 847 (2023), DOI:10.1134/S0021364023603329

32. I. O. Kulik, Sov. Phys. JETP **30**, 944 (1970).

33. P. Dubos, H. Courtois, B. Pannetier, F. K. Wilhelm, A. D. Zaikin, and G. Schön, Phys. Rev. B **63**, 064502 (2001)

34. A. M. Toxen, Phys. Rev. 123, 442 (1961).

35. P. Scharnhorst, Phys. Rev. B **1**, 4295 (1970).

36. K. K. Likharev, Rev. Mod. Phys. **51**, 101 (1979).

37. I. Sochnikov, L. Maier, C. A. Watson, J. R. Kirtley, C. Gould, G. Tkachov, E. M. Hankiewicz, C. Brune, H. Buhmann, L. W. Molenkamp, and K. A. Moler, Phys. Rev. Lett. **114**, 066801 (2015)

38. E. Bocquillon, J. Wiedenmann, R. S. Deacon, T. M. Klapwijk, H. Buhmann, and L. W. Molenkamp, *Microwave Studies of the Fractional Josephson Effect, HgTe-Based Josephson Junctions*, in: *Topological Matter*, ed. by D. Bercioux, J. Cayssol, M. Vergniory, and M. Reyes Calvo, Springer Series in Solid-State Sciences, Vol. 190, Springer (2018).

39. C. Vanneste, C. C. Chi, W. J. Gallagher, A. W. Kleinsasser, S. I. Raider, and R. L. Sandstrom, J. Appl. Phys. **64**, 242 (1988), DOI:10.1063/1.341471

40. R. C. Dinsmore III, Myung-Ho Bae, and A. Bezryadin, Appl. Phys. Lett. **93**, 192505 (2008), DOI:10.1063/1.3012360

41. A. Valizadeh, M. R. Kolahchi, and J. P. Straley, J. Nonlinear Math. Phys. **15**, 407 (2008).

42. S. M. Frolov, D. J. Van Harlingen, V. V. Bolginov, V. A. Oboznov, and V. V. Ryazanov, Phys. Rev. B **74**, 020503 (2006).

43. L. Chen, P. Chen, and C. K. Ong, Appl. Phys. Lett. **80**, 1025 (2002).

44. A. Leblanc, C. Tangchingchai, Z. Sadre Momtaz, E. Kiyooka, J.-M. Hartmann, F. Gustavo, J.-L. Thomassin, B. Brun, V. Schmitt, S. Zihlmann, R. Maurand, E. Dumur, S. De Franceschi, and F. Lefloch, arxiv:2405.14695

45. S. Messelot, N. Aparicio, E. de Seze, E. Eyraud, J. Coraux, K. Watanabe, T. Taniguchi, and J. Renard, arxiv:2405.13642

46. L. Banszerus, C. W. Andersson, W. Marshall, T. Lindemann, M. J. Manfra, C. M. Marcus, and S. Vaitiekenas, arxiv:2406.20082